

ICCC 2023 - Guidelines for citation and reuse



Please cite the conference proceedings as following:

Thailand Concrete Association, Ed. *Further Reduction of CO₂ -Emissions and Circularity in the Cement and Concrete Industry, 16th International Congress on the Chemistry of Cement 2023 - ICC2023* (Bangkok 18.-22.09.2023). Bangkok, 2023. Available at: <https://www.iccc-online.org/archive/>

Please cite individual papers as following:

Author. Title. In: Thailand Concrete Association, Ed. *Further Reduction of CO₂ -Emissions and Circularity in the Cement and Concrete Industry, 16th International Congress on the Chemistry of Cement 2023 - ICC2023* (Bangkok 18.-22.09.2023). Bangkok, 2023. Available at: <https://www.iccc-online.org/archive/>

All papers in the 2023 conference proceedings are published under the license CC-BY-ND 4.0.

(<https://creativecommons.org/licenses/by-nd/4.0/legalcode>)



Organized by
TCA
สมาคมคอนกรีตแห่งประเทศไทย
Thailand Concrete Association

THE CHEMISTRY OF CEMENT • THE 16TH INTERNATIONAL CONGRESS ON
**ICCC
2023**
BANGKOK
THAILAND



ICCC ^{16th} **2023**
INTERNATIONAL CONGRESS ON THE CHEMISTRY OF CEMENT

CONGRESS PAPER **VOLUME I**

Further reduction of CO₂-emission
and circularity in the cement and concrete industry

SEPTEMBER 18-22, 2023

CENTARA GRAND & BANGKOK CONVENTION CENTRE @CENTRALWORLD

Co-Sponsor by



Contact information :

Email: iccc2023.tca@gmail.com

Website : <https://www.iccc2023.org/>

Contents

	Topics	Page
	Preface	i
	Committees	
	- Steering Committee Members	ii
	- Organizing Committee Members	iii
	- Scientific Committee Members	v
	Papers	
PA0001	Effect on Graphene Oxide and Silica Fume on the Performance of Concrete under Standard Curing Conditions	1
PA0008	Comparison of the mode of action of a shotcrete accelerator in a slag cement and an OPC cement	5
PA0009	3D-printable magnesium-silicate-hydrate cement composites: A feasibility study	9
PA0010	Evaluation of Internal Cracks and Three-Dimensional Deformation due to Different Nozzle Paths in a Material Extrusion 3D Printer	13
PA0012	Use of volcanic ash in an ECC material for 3D printing	18
PA0013	Future projection of carbon dioxide emission in calcium carbonate concrete (CCC) production	22
PA0015	Novel Soluble Boron Compounds to Improve Shielding of Cement Systems	26
PA0016	Constructing solutions using cement-based materials for energy harvesting and storage	30
PA0020	Use of biomass ash in the fabrication of Self-healing engineered cementitious composites (ECC)	34
PA0021	Assessment of early-age drying induced microstructural changes in 3D printed cement mortar	38
PA0025	3D Printing Mortar and Concrete: Advancement and Application of Laboratory Test Protocol to Evaluate Properties physicochemical and mechanical.	42
PA0028	The Role of Belitic Calcium Sulfoaluminate Cement in Achieving Net-zero	46
PA0035	Carbon neutral concrete based on a sea snail shell: a green solution for the urban heat island	50
PB0001	Prediction of Total Bond Order Density of Cement Crystals using Fermionic Hubbard Model and Bloch and Fermi Surface	54

Contents

	Topics	Page
PAPERS		
PB0002	Digitalization in cement production: prediction of free lime content in clinker production	58
PB0003	Method of Intensifying Cement Clinker Production	62
PB0004	Piezoresistive performance of GNP-modified highly deformable cementitious materials	66
PB0007	Research on the preparation of low-calcium Portland cement	70
PB0008	Determination of Clinker Performance with Chemical Additives by use of XRF, QXRD and Microscopy Analysis.	74
PB0009	Preparation and Characterization of Portland cement Clinker by High Magnesium Limestone and Iron Tailings	78
PB0010	Production and Analysis of BYF Clinker Produced via the Combustion of Elemental Sulfur	82
PB0015	Effect of cooling rates on the properties of Portland cement clinkers in the presence of Mg	86
PB0016	Effect of chlorides on the clinkering and reactivity of ye'elimite	90
PB0017	Effect of Synthesis Conditions, Zn Doping and Al/Fe Ratio on Calcium [Alumino] Ferrite Structure	94
PC0002	Recent advances in understanding the hydration of limestone calcined clay cements (LC ³)	98
PC0003	Microstructural mechanism involved in the expansion generated in cementitious materials with expansive agent type K	105
PC0011	The influence of free water removal approaches on the composition and morphologies of CAC hydrates cured at different temperatures	109
PC0016	Effect of temperature rise inhibitor on heat evolution of cement-quartz system	113
PC0020	Influence of ferronickel slag on early hydration and microstructure of alkali-activated ground granulated blast furnace slag	117
PC0022	Synthesis and characterization of iron and aluminium-containing AFm phases	122
PC0024	Effect of titanium dioxide nanoparticles on hydration and mechanical properties of mortar based on a ternary binder system	126

Contents

	Topics	Page
PAPERS		
PC0025	Role of Gypsum on Early Age Hydration of Alite Polymorphs (TI and TIII): A Temporal X-ray PDF Analysis	130
PC0026	Adsorption of Ca^{2+} at Micro Aggregate Surface and Its Effect on Particle Interaction, C-S-H Formation and Adhesion	134
PC0027	In Situ X-ray Total Scattering Study on the Impact of Gypsum in C3S-Metakaolin-Limestone Systems	138
PC0029	Hydration of CAC pastes at high temperature	142
PC0031	A Combined Calorimetry and XRD Study of The First 15 Minutes of Portland Cement Hydration	146
PC0037	Comparative study of the hydration kinetics of oil well cement and model cement retarded by tartaric acid at elevated temperatures	150
PC0039	Hydration of tricalcium aluminate-sulphate systems in presence of alkanolamines	154
PC0040	Thermogravimetric analysis on the effect of SAP addition on the microstructure of cement based materials	158
PC0042	Sodium sites and hydration state in C-S-H phases synthesized under alkaline conditions from ^1H and ^{23}Na MAS NMR experiments	162
PC0043	Effect of irradiation on Portland cement pastes: impact on mineralogy, mechanical properties, and microstructure	166
PC0044	Influence of TiO_2 on the kinetic reaction of white Portland cement suspensions	170
PC0046	Early hydration and rheological behavior of the calcium aluminates mixtures in the presence of gypsum	171
PC0048	Elucidation of hydration reaction of blended OPC by the utilization of alkanolamine-base grinding agent	176
PC0049	An insight on the effect of KAlO_2 on hydration kinetics and mechanical properties of ternesite	179
PC0050	Synthesis of sodium iron silicate hydrate (N-F-S-H)	183
PC0052	Nucleation of C-S-H from Molecular Dynamics	187
PC0053	Study of early age hydration behavior of sulfate-rich belite sulfoaluminate cements with anhydrite and gypsum	191
PC0054	Identification of Phases in Cementitious Materials at Critical Elevated Temperatures	196

Contents

	Topics	Page
PAPERS		
PC0055	Time resolved synchrotron X-ray diffraction investigations of LC3 hydration in the presence of hydroxyethyl methyl cellulose ethers	200
PC0056	Mineral dissolution mechanism of different polymorphs of alite from ReaxFF molecular dynamics simulation	204
PC0058	Hydration of Calcium [Alumino] Ferrite with Limestone	209
PC0059	Deciphering the defects of alite particles at the single-atom level	213
PC0077	The Influence of Aluminum Uptake on the Mechanical Properties of Calcium Silicate Hydrate	217
PD0001	New steel production processes and their consequences for slag utilization in cement	221
PD0003	The effect of iron phases on the performance of calcined clays in calcined clay-limestone cement	225
PD0005	Dilution Effects in Cementitious Matrices by Using Calcined Clay and Limestone for Reduced Clinker Factors	229
PD0006	Study on Calcined Clay-Recycled Concrete Powder Composite as Supplementary Cementitious Material	233
PD0007	Study of filler effect of VGP on cement hydration	238
PD0008	Reactivity of alternative supplementary cementitious materials assessed by the R ³ method	243
PD0009	Activation of LC ³ low-carbon cements by C-S-H seeding	247
PD0012	Nucleation Effects of Biologically Architected Calcium Carbonate in Portland Limestone Cements	251
PD0014	Dune sand powders characterization for their use in cement-based materials	258
PD0019	Pore structure refinement of calcium-sulfate-aluminate--Portland cement mortars by early-age CO ₂ curing	262
PD0021	Simulation of sulfate attack on carbonated Portland cement-blast furnace slag binary cement	266
PD0022	A Study on Hydration Properties of Cement Matrix according to Limestone Content for Portland Cement	270
PD0023	Mineralogical analysis of BOF slag with different grinding characteristics	274
PD0026	Cement Hydration Kinetics of LC3 Paste Synthesized with Biologically Architected CaCO ₃	278

Contents

	Topics	Page
PAPERS		
PD0029	Effect of silica fume on long-term hydration and compressive strength of UHPC under different curing regimes	282
PD0033	Variation of Fluidity of Calcined Clay Limestone Cements by Power Ultrasound and Gypsum Addition	286
PD0034	Effect of solid wastes with different activities on the rheological properties of 3D printing low carbon concrete	291
PD0035	Assessing the activity of potential SCM's using the R3 test method	295
PD0036	The effect of ionic environment of cement pore solution on the PCE's molecular conformation, adsorption and performance	299
PD0040	Performance of calcined anthill clay as a supplementary cementitious material	304
PD0042	Reactivity of alternative SCMs from Nordic Countries – Input for the R ³ test	309
PD0043	New Insights on the Use of Sewage Sludge Ashes as Supplementary Cementitious Materials	313
PD0044	Impact of Ca/Si and Al/Si ratio on the alumina-silica gel formed by wet carbonation of synthesized C-S-H phases	317
PD0045	About The Effect Of Portland Cement Activation On Supersulfated Cements Properties	321
PD0046	Determining the reaction kinetics of supplementary cementitious materials for input into thermodynamic-kinetic models	325
PD0048	Characterization of (A/F) H ₃ Phase Microstructure with Different Al/(Fe+Al) Ratios based on Calcium Sulfoaluminate Cement	329
PD0052	Restraining strength retrogression of silica-cement at high temperature above 200 °C using flint clay and graphite	333
PD0054	Influence of mineralogical composition on the calcinability of shales	338
PD0055	A New Soluble Alkali Test to Predict the Alkali Contribution of SCMs to Concrete Pore Solution	343
PD0056	Sensitivity of the Modified Chapelle test for measuring the reactivity of different types of clays calcined under different conditions	347

Contents

	Topics	Page
PAPERS		
PD0057	Use of alkaline salts to improve the reactivity of cements with high fly ash content: hybrid alkaline cements	351
PD0059	Reduced OPC content in limestone calcined clay cement (LC ³) with C-S-H seeding	356
PD0061	Novel strength enhancing cement additives to enable production of low-clinker cements	360
PD0062	How siderite (FeCO ₃) might be a future low-CO ₂ reactive binder component for composite cements	365
PD0063	A Particle Packing Approach for Eco-efficient Ultra High-Performance Concrete (E-UHPC)	369
PD0065	Production of Low-Heat Cement from Industrial Waste	373
PD0067	Hydration of ternary blended cements comprising co-calcined bauxite residue and kaolinitic clay	377
PD0068	Effect of chloride salts on cement hydration: influence of the cation - part II	381
PD0070	Correlating initial chemistry, reaction degree and phase assemblage in alkali-activated systems	385
PD0071	Preliminary Selection Criteria of Clays for Limestone Calcined Clay Cement	389
PD0078	Scientific dosage of self-compacting concretes containing ternary cement mixtures	393
PD0079	Impact of curing time on carbonation of low-clinker binders	397
PD0080	Effect of Admixture for Slag on the Strength Development of Cement blend containing Cement, Slag, and Calcium Carbonate	401
PD0081	Refinement of activation methods for increased reactivity of kaolinitic and illitic clays	405
PD0082	Effect of temperature on the heat of hydration and compressive strength of ternary blends	409
PD0090	Alkali-carbonate activated waste glass-based cements	413
PD0091	Alkali-activation and chemical stabilization of incineration fly ash using slag for dangerous waste storage	417
PD0095	Impact of calcination technology on the properties of a low kaolinite calcined clay	421
PD0096	Fresh and hardened state properties of ternary slag cement concrete with high filler content	425

Contents

	Topics	Page
PAPERS		
PD0097	LC ³ application in Non-structural Concrete	429
PD0099	Functionalization of Metakaolin with Non-Ionic Surfactants: Swelling and Pozzolanic Reactivity	433
PD0101	Reactivity (R ³) and hydration products of Fe(II)-rich slags: from CaO-FeO _x -SiO ₂ to CaO-Al ₂ O ₃ -Na ₂ O-FeO _x -SiO ₂	437
PD0104	Bauxite residue as a new source of SCM: its impact on cement hydration and interaction with fly ash	441
PD0108	Development of supplementary cementitious materials using weathered volcanic eject	445
PD0110	Beyond kaolinite content: untangling the influence of other clay properties on the reactivity of calcined clays	449
PD0111	Use Of Supplementary Cementitious Materials For Composite Cements: An Overview	453
PD0113	Application of Interparticle Spacing Model to Maximize Filler Content in Cementitious Pastes	457
PD0115	Effects of Blast Furnace Slag Fineness on Cement Physical, Mechanical and Chemical Properties	461
PD0118	Improving early-age strength of limestone-calcined clay cement by using finer cement and cement kiln dust	465
PD0122	Alkali-activated fly ash synthetized with pre-polymerized suspension combined with ultrafine fly ash at ambient temperature	469
PD0123	A unified method for efficient and reliable determination of pozzolanic reaction degree of SCMs in blended cement pastes	473
PD0124	Power ultrasound assisted production of sustainable concrete	477
PD0125	Feasibility of using volcanic debris from the island of La Palma as building materials	481
PD0127	Blended systems with OPC-Pozzolan-High limestone filler	485
PD0131	Relationship between reactive alumina content of Calcined Clays and fresh cement pastes behaviour.	489
PD0133	Quantitative microstructure analysis of SCM-blended cementitious materials through deep learning-based computer vision methods	494
PD0134	Effect of steam curing on the hydration of limestone calcined clay cements (LC ³) with low kaolinite content	498

Contents

	Topics	Page
PAPERS		
PE0002	Relationship between rate of hydration and physical and chemical characteristics of Portland cement	502
PE0003	Combined use of laboratory X-ray diffraction and microtomography in early age cement hydration	512
PE0004	Characterization of siliceous hydrogarnet ($\text{Ca}_3\text{Al}_2(\text{SiO}_4)_x(\text{OH})_{12-4x}$) by solid-state NMR spectroscopy	516
PE0006	Influence of MgO on formation of clinker with different alumina modulus based on big data	520
PE0007	Multiscale investigation on the thermal stability of synthetic C-S-H pastes according to Ca/Si ratios	524
PE0008	Molecular dynamics on the pressure exerted by water molecules confined in microporous C-S-H	528
PE0009	Investigation of Selective Dissolution Method for Separation of Ferrite Phase in Cement and Characterization	532
PE0010	A comparative study of tribometer rotor configurations and analytical methods for concrete pumping pressure prediction	536
PE0011	Microstructural analysis of the effect of clinker phase distribution on cement hydration using computer-based approaches	540
PE0012	Application of artificial intelligence on the reconstruction of multi-phase cement paste microstructures	543
PE0013	Numerical Model for Growth and Porosity of C-S-H Structures in Cement Hydration	547
PE0014	Micromechanical properties of C-A-S-H and C-A-S-H/CH mixtures based on nanoindentation	551
PE0015	Methods for measuring internal stress and expansion deformation of fresh concrete during steam curing	555
PE0019	Mineralogical Investigation of Coal Fly Ash using Combined SEM-EDS and Raman Spectroscopy	559
PE0020	Study of alite and belite dissolution by kinetic Monte Carlo simulations and its effect in cement hydration.	563
PE0022	Machine learning atomic potential for C-S-H	567
PE0023	Assessment of Radiation-Induced Degradation in a Siliceous Rock via Correlative Characterization	571

Contents

	Topics	Page
PAPERS		
PE0024	Solid state NMR study of the hydration of a fast-setting ternary binder added with lithium carbonate or trisodium-citrate	575
PE0025	Exploring C-S-H clusters with evolutionary algorithms	579
PE0027	Structure and mechanical properties of calcium silicate hydrate and calcium carbonate nano composites resolved by reactive molecular dynamics simulations	583
PE0029	MD study of radiocesium immobilization in the geopolymer matrix	587
PE0031	Modelling of the Flocculated Polydisperse Microstructure of Fresh Cement Paste	591
PE0037	Simulation of heat transport in extruded concrete structure	595
PE0042	In situ monitoring of microstructure evolution of C3A – gypsum system by low field NMR	599
PE0045	Thermodynamic modelling of Portland cement clinkers.	603
PE0048	Calcium Silicate Hydrate Surface	607
PE0050	Experimental thermodynamic study of selected cement clinker phases	611
PE0052	Atomic Scale Insight of Hydration Temperature Rise Inhibitors (TRI) Affecting Calcium Activity via AIMD	615
PE0053	Impact of autoclaving on the phase assemblage of Portland cement: Experiment and thermodynamic modelling	619
PE0054	A Multi-scale Model of Reinforcement Bars Corrosion Based on the Concentrated Electrolyte Theory and Three Dimensional Hierarchical Structure of Concrete	623
PE0057	Multi-scale model for characterizing thermal conductivity of cement-based materials with nano inclusions	628

Impact of autoclaving on the phase assemblage of Portland cement: Experiment and thermodynamic modelling

T. Hirsch^{1,*}, M. Voigt², C. Lehmann¹, B. Meng², and B. Lothenbach^{3,4}

¹ Technische Universität Berlin, Faculty VI Planning Building Environment, Building Materials and Construction
Chemistry, Berlin, Germany
Email: t.hirsch@tu-berlin.de, c.lehmann@tu-berlin.de

² Bundesanstalt für Materialforschung und -prüfung, Fachbereich 7.1 Baustoffe, Berlin, Germany
Email: marieke.voigt@bam.de, birgit.meng@bam.de

³ Empa, Concrete & Asphalt Laboratory, Dübendorf, Switzerland

⁴ NTNU, Department of Structural Engineering, Trondheim, Norway
Email: barbara.lothenbach@empa.ch

ABSTRACT

Even after autoclaving for 2 weeks in the temperature range of 120 to 200 °C, CEM I paste with a water-to-cement ratio of 0.5 still contains some low-crystalline C-S-H. The conversion of low-crystalline C-S-H to crystalline is faster with increasing temperature. The observed low-crystalline and crystalline C-S-H phases (reinhardbraunsite, jaffeite) indicate that the samples have not reached equilibrium yet under these experimental conditions. However, there is a good agreement between experiment and thermodynamic modelling for the other solids indicating that the used datasets are suitable for this application.

KEYWORDS: Autoclaving, Crystalline C-S-H, Scawtite, Hydroxyllestadite

1. Introduction

When concrete is exposed to hydrothermal conditions beyond 100 °C, the phase assemblage changes substantially (Werder et al. 2021; Tian et al. 2022). Such conditions are typically applied in the production of autoclaved (aerated) concrete, calcium silicate bricks and other autoclaved calcium silicate building products (Society of Chemical Industry 1967; Kikuma et al. 2009). The low-crystalline C-S-H gel observed at room temperature is replaced by crystalline C-S-H phases. Sulfate is bound in calcium sulfates or hydroxyllestadite. Depending upon the system chemistry, portlandite and hydrogarnet may occur. Thermodynamic modelling is frequently performed for temperatures below 100 °C and has strongly enhanced the understanding of cement hydration and deterioration (Lothenbach and Zajac 2019). Beyond 100 °C, however, thermodynamic data for hydrated cements is lacking. The current publication compares experimental observations for a CEM I paste with predictions made by the combination of thermodynamic datasets commonly used in cement science with the recent dataset of Hirsch et al..

2. Materials and methods

The oxide composition of the CEM I 52.5 R (Dyckerhoff) used was determined by X-ray fluorescence (XRF) using a WD-RFA PW 2400 (Philips) based on powder tablets as well as fused discs. Water and carbon dioxide were quantified by thermogravimetric analysis (TG) using a TG2 09 F3 Tarsus (Netzsch) heating at 10 °C/min from room temperature to 850 °C in a nitrogen atmosphere with a flow rate of 40 mL/min. The results are presented in Table 1.

Table 1: Oxide composition of used CEM I as determined by XRF and TG.

Al ₂ O ₃	CaO	Fe ₂ O ₃	K ₂ O	MgO	MnO	Na ₂ O	P ₂ O ₅	SiO ₂	SO ₃	TiO ₂	CO ₂	H ₂ O	Sum
3.64	66.24	1.44	0.6	0.91	0.04	0.3	0.16	21.78	2.72	0.21	1.57	0.86	100.47

Cement paste was prepared at a water-to-cement ratio of 0.5 using a planetary centrifugal mixer. The paste was filled in cylindrical molds of 22.6 by 22.6 mm, covered with foil, and stored at 23 °C and 50% relative humidity for 24 h. After demolding, the samples were autoclaved at the target temperatures (120 to 200 °C in 20 K increments) for 14 days under saturated water vapor pressure and, after this, cooled in the autoclave to room temperature. Subsequently, the samples were crushed, ground with isopropanol in a McCrone mill and dried under vacuum at 40 °C for 2 days. The powder samples were mixed with an internal standard (10 wt% of ZnO). X-ray diffraction was performed with a Bragg-Brentano diffractometer (Empyrean, PANalytical). The Cu K α radiation was generated with 40 kV and 40 mA, filtered by Ni and measured by a PiXcel^{1D}. For phase quantification, Rietveld refinements were performed using HighScore Plus 4.8. The structure data used for the refinements was taken from ICSD and is listed in Table 2.

Table 2: Phases with ICSD structure numbers used for Rietveld refinements.

Alite	22501	Portlandite	73467
Tricalcium aluminate	1880	Hydroxyllellstadite	39775
Hydrogarnet (larger unit cell)	49772	Jaffeite	39725
Hydrogarnet (smaller unit cell)	172076	Reinhardbraunsite	200924
Calcite	166364	ZnO	155780

The thermodynamic modelling was conducted using the thermodynamic software GEMS (Kulik et al. 2012; Wagner et al. 2012) version 3.7. The databases PSI/Nagra 12/07 (Thoenen and Kulik 2003; Thoenen et al. 2014), Cemdata18 (Lothenbach et al. 2019) and datasets for zeolites (Ma and Lothenbach 2020a, 2020b) provided basic thermodynamic properties. Furthermore, the database cCSH for crystalline C-S-H and some additional phases forming at elevated temperatures and pressures (Hirsch et al.) was included. As the datasets of Ma and Lothenbach contain data for zeolites, the zeolites of Cemdata18 were deactivated for internal consistency. The species $\text{Si}_4\text{O}_8(\text{OH})_4^{4-}$ of PSI/Nagra was deactivated as its data are only reliable for ambient conditions.

3. Results

The experimental results are presented in Figure 1. Despite a dwell time of 2 weeks, the samples autoclaved at 120 to 160 °C still contain small quantities of clinker phases, which diminish with rising temperature.

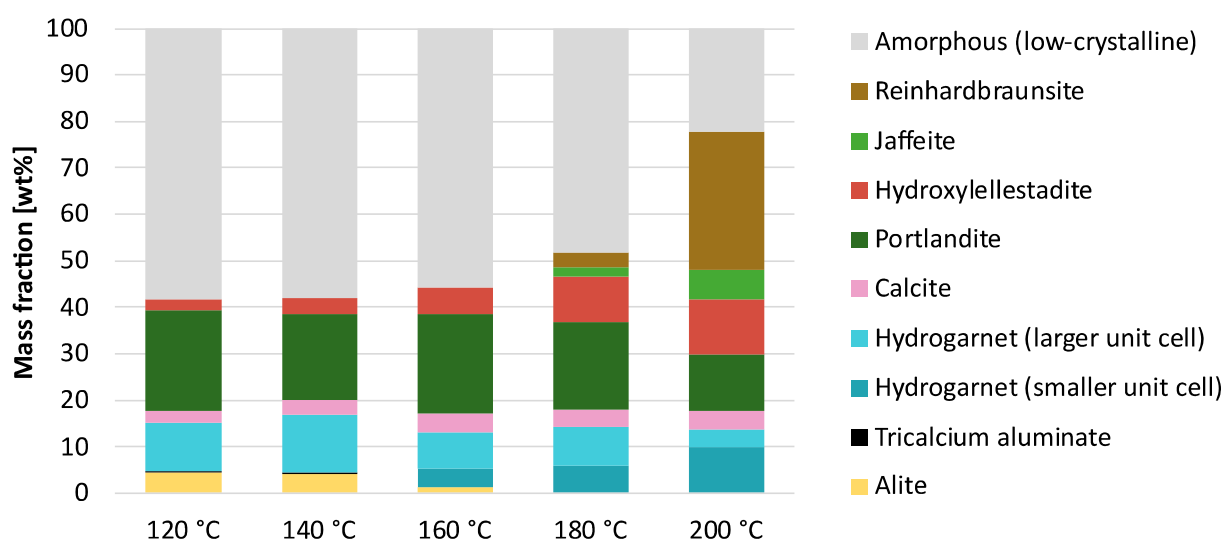


Figure 1: Solid phase assemblage in autoclaved pastes as determined by Rietveld refinement.

In general, the samples are quite similar in their phase assemblage. Nevertheless, a splitting of the hydrogarnet reflexes in XRD occurs in the temperature range between 140 and 160 °C, which persists at higher temperature. The summed share of the two hydrogarnets varies however only slightly between all samples. The share of calcite is nearly constant and increases only very slightly between 120 and 160 °C.

Further phases present in all samples are a low-crystalline phase (very likely C-S-H), portlandite and hydroxyllellstadite. At lower temperatures, the low-crystalline C-S-H accounts for more than half of the sample. In the samples autoclaved at 180 and 200 °C, the two crystalline C-S-H phases reinhardbraunsite and jaffeite appear. While their share is still small at 180 °C, both, in particular reinhardbraunsite, gain at 200 °C while the portion of low-crystalline C-S-H diminishes. Simultaneously, a strong increase in the quantities of hydroxyllellstadite and decrease of portlandite can be observed. Both of these effects are likely due to the reaction of low-crystalline C-S-H, which liberates the sulfate adsorbed on its large surface (Barbarulo et al. 2007). The destabilization of low-crystalline C-S-H leads consequently to release of sulfate, which is bound in hydroxyllellstadite. Portlandite is likely consumed as the formation of reinhardbraunsite and jaffeite from low-crystalline C-S-H requires additional Ca.

Thermodynamic modelling predicts the formation of hillebrandite in the whole temperature range and metaettringite around 200 °C. Ettringites are known to be low temperature phases (Zhou and Glasser 2001), indicating an overestimation of the metaettringite stability at 200°C. Hillebrandite was not observed in the current experiments, and is known to form very slow or not at all depending on the experimental conditions (Garbev 2004). Consequently, both phases were deactivated in the modelling. The resulting thermodynamic models are qualitatively quite close to the experiment (Figure 2). The existence of portlandite, hydrogarnet, hydroxyllellstadite and a small quantity of calcite agrees well with the experimental observations. The modelling even predicts the formation of two individual hydrogarnets indicating that the persistence of one sole hydrogarnet in the low-temperature samples may be due to kinetic reasons. Hydrotalcite and pyrolusite are predicted as well but not observed experimentally, which might be due to their small quantities and potentially low crystallinity (pyrolusite is not visible in Figure 2 due to low quantity). In experiment and simulation, the phase assemblage is dominated by C-S-H phases. The low-crystalline C-S-H in the experiment is likely metastable as:

- Experiments in the literature show that increase in dwell time and water content yield in more crystalline C-S-H phases
- Thermodynamic modelling predicts crystalline C-S-H (Figure 2)
- At higher temperature, the low-crystalline C-S-H decreases in quantity and crystalline C-S-H phases form, which occur in the thermodynamic predictions (Figure 1)

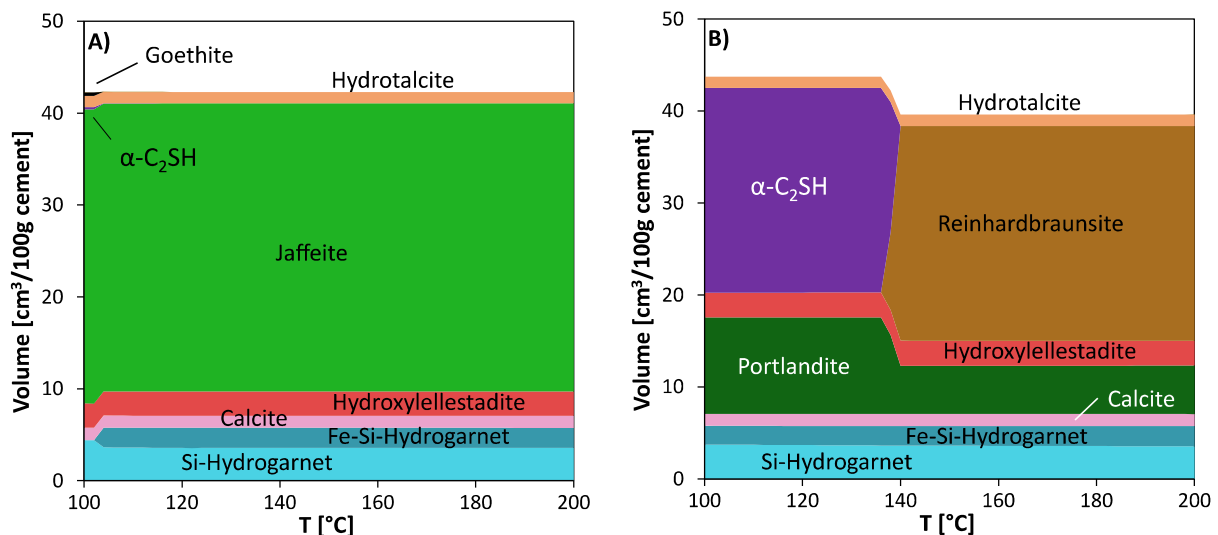


Figure 2: Thermodynamic modelling of the phase assemblage in autoclaved CEM I paste. A) with suppressed formation of metaettringite and hillebrandite, B) with suppressed formation of metaettringite, hillebrandite and jaffeite.

Hillebrandite formation seems to be kinetically hindered in the experiments. If hillebrandite is suppressed in the modelling, the formation of jaffeite is predicted but not of reinhardbraunsite. Reinhardbraunsite is only predicted if also jaffeite is prohibited to form. The samples at higher temperature possess higher shares of reinhardbraunsite than jaffeite. This could be interpreted in the way that reinhardbraunsite forms faster

than jaffeite (and hillebrandite) under the experimental conditions, potentially because less portlandite is required for the reaction of low-crystalline C-S-H to reinhardbraunsite than is needed for the reaction to jaffeite.

4. Conclusions

Combining several thermodynamic databases, the experimentally observed phase assemblage of a CEM I paste exposed to autoclaving was modelled successfully. Experimental results and modelling indicate that the C-S-H phases are still far from equilibrium after 2 weeks. Crystalline C-S-H phases were not observed in samples autoclaved between 120 and 160 °C. The other phases are found in the experiment as predicted by thermodynamic modelling disregarding minor phases. Further comparison studies between experimental work and thermodynamically predicted phase assemblages should be undertaken to test and refine the datasets.

Acknowledgements

The authors are grateful for founding of this work by German Federal Ministry of Economic Affairs and Energy in scope of the project “BeHeWaDS” (03ET1537A).

References

- Barbarulo, R.; Peycelon, H.; Leclercq, S. (2007): Chemical equilibria between C–S–H and ettringite, at 20 and 85 °C. In *Cem. Concr. Res.* 37 (8), pp. 1176–1181. DOI: 10.1016/j.cemconres.2007.04.013.
- Garbev, K. (2004): Struktur, Eigenschaften und quantitative Rietveldanalyse von hydrothermal kristallisierten Calciumsilikathydraten (C-S-H-Phasen). Forschungszentrum Karlsruhe in der Helmholtz-Gemeinschaft, Wissenschaftliche Berichte FZKA 6877. Doctoral thesis. Ruprecht-Karls-Universität Heidelberg, Heidelberg. Institut für Technische Chemie.
- Hirsch, T.; Lothenbach, B.: Phase stabilities and thermodynamic properties of crystalline CaO–SiO₂–H₂O phases above 100 °C (to be submitted).
- Kulik, D.A.; Wagner, T.; Dmytrieva, S.V.; Kosakowski, G.; Hingerl, F.F.; Chudnenko, K.V.; Berner, U.R. (2012): GEM-Selektor geochemical modeling package: revised algorithm and GEMS3K numerical kernel for coupled simulation codes. In *Comput. Geosci.* 26 (012025), p. 189. DOI: 10.1007/s10596-012-9310-6.
- Lothenbach, B.; Kulik, D.A.; Matschei, T.; Balonis, M.; Baquerizo, L.; Dilnesa, B. et al. (2019): Cemdata18: A chemical thermodynamic database for hydrated Portland cements and alkali-activated materials. In *Cem. Concr. Res.* 115, pp. 472–506. DOI: 10.1016/j.cemconres.2018.04.018.
- Lothenbach, B.; Zajac, M. (2019): Application of thermodynamic modelling to hydrated cements. In *Cem. Concr. Res.* 123, p. 105779. DOI: 10.1016/j.cemconres.2019.105779.
- Ma, B.; Lothenbach, B. (2020a): Synthesis, characterization, and thermodynamic study of selected Na-based zeolites. In *Cem. Concr. Res.* 135, p. 106111. DOI: 10.1016/j.cemconres.2020.106111.
- Ma, B.; Lothenbach, B. (2020b): Thermodynamic study of cement/rock interactions using experimentally generated solubility data of zeolites. In *Cem. Concr. Res.* 135, p. 106149. DOI: 10.1016/j.cemconres.2020.106149.
- Thoenen, T.; Hummel, W.; Berner, U.; Curti, E. (2014): The PSI/Nagra Chemical Thermodynamic Database 12/07. PSI report 14-04. Edited by Nuclear Energy and Safety Research Department Laboratory for Waste Management (LES). Paul Scherrer Institut (PSI). Villigen, Switzerland.
- Thoenen, T.; Kulik, D. (2003): Nagra/PSI Chemical Thermodynamic Data Base 01/01 for the GEM-Selektor (V.2-PSI) Geochemical Modeling Code: Release 28-02-03. Internal Report TM-44-03-04. Edited by Paul Scherrer Institut (PSI). Available online at <http://gems.web.psi.ch/TDB/doc/pdf/TM-44-03-04-web.pdf>.
- Tian, H.; Hirsch, T.; Stephan, D.; Lehmann, C. (2022): The Influence of Long-Term Autoclaving on the Properties of Ultra-High Performance Concrete. In *Front. Mater.* 9, Article 844268, p. 38. DOI: 10.3389/fmats.2022.844268.
- Wagner, T.; Kulik, D.A.; Hingerl, F.F.; Dmytrieva, S.V. (2012): GEM-Selektor geochemical modeling package: TSolMod library and data interface for multicomponent phase models. In *Can. Mineral.* 50 (5), pp. 1173–1195. DOI: 10.3749/canmin.50.5.1173.
- Werder, J. von; Simon, S.; Gardei, A.; Fontana, P.; Meng, B. (2021): Thermal and hydrothermal treatment of UHPC: influence of the process parameters on the phase composition of ultra-high performance concrete. In *Mater Struct* 54 (1), p. 250. DOI: 10.1617/s11527-021-01633-w.
- Zhou, Q.; Glasser, F.P. (2001): Thermal stability and decomposition mechanisms of ettringite at <120°C. In *Cem. Concr. Res.* 31 (9), pp. 1333–1339. DOI: 10.1016/S0008-8846(01)00558-0.